Towards an Analysis of Shear Suspension Flows Using Radial Basis Functions

K. Le-Cao[1], N. Mai-Duy[1], C.-D. Tran[1] and T. Tran-Cong[1]

Abstract: In this paper, radial basis functions are utilised for numerical prediction of the bulk properties of particulate suspensions under simple shear conditions. The suspending fluid is Newtonian and the suspended particles are rigid. Results obtained are compared well with those based on finite elements in the literature.

Keywords: Integrated radial basis functions; Multiphase flows; Shear boundary conditions; Bulk properties.

1   Introduction

Particulate suspensions, which involve transport of rigid particles suspended in a fluid medium, occur in many industrial processes such as slurries, colloids, fluidised beds, etc. Due to their great structural and physical variety, the use of experiments to determine the macroscopic rheological properties of these multiphase materials was seen to be impractical [Phan-Thien and Kim (1994)]. However, it may be possible to employ numerical simulations to predict the bulk properties of multiphase materials. Various numerical models have been proposed. Among them, direct numerical simulations (DNSs), which consist in solving the fundamental equations for particles (Newton-Euler equation) and a fluid (Navier-Stokes equation) in a direct and fully-coupled manner, have received a great deal of attention. Two main advantages of DNSs are that (i) they can handle particles of different shapes and sizes as well as any type of fluid and (ii) hydrodynamic forces and moments can be calculated directly from the fluid flow. Difficulties faced by DNSs include (i) a very large number of particles is typically required for a proper simulation and (ii) the fluid domain is of very complex shape due to the presence of particles and the change of their positions with time. Based on the fluid-phase solver employed, DNSs can be classified into two categories. In the first category, a mesh follows the movement of the particles, i.e. a moving mesh is used. Methods based

---

[1] Computational Engineering and Science Research Centre (CESRC), Faculty of Engineering and Surveying, University of Southern Queensland, Toowoomba, QLD 4350, Australia.

on the arbitrary Lagrangian-Eulerian (ALE) moving mesh approach proposed by Hu, Joseph, and Crochet (1992) are widely used, e.g. [Hu (1995); Huang, Feng, Hu, and Joseph (1997); Huang, Hu, and Joseph (1998)]. In the second category, a mesh covers the whole domain and is independent of the position of particles, i.e. a fixed mesh is used. Methods based on the fictitious domain approach proposed by Glowinski, Pan, and Periaux (1998) are widely employed, e.g. [Hwang, Hulsen, and Meijer (2004); Patankar, Singh, Joseph, Glowinski, and Pan (2000); Singh, Joseph, Hesla, Glowinski, and Pan (2000)]. Hwang, Hulsen, and Meijer (2004) incorporated sliding bi-periodic frames, introduced by Lees and Edwards (1972) for molecular dynamics, into the simulation of particulate flows. This concept allows the modelling of suspension systems with infinite numbers of particles to be conducted through a small number of particles in a representative reference sliding frame. The computational fluid domain is thus small with bi-periodic conditions on the frame and no-slip conditions on the surfaces of the particles.

Over the last two decades, radial basis functions (RBFs), proven to be universal approximators, have been developed and applied to solve different types of differential problems encountered in applied mathematics, science and engineering, e.g. [Fasshauer (2007); Kansa (1990); Le-Cao, Mai-Duy, and Tran-Cong (2009); Sarler (2005)] and the references therein. RBF-based methods are extremely easy to implement and capable of achieving a high level of accuracy using a relatively-small number of nodes. One can construct RBF-based approximations through differentiation or integration. Since integration is a smoothing operator, the latter has higher approximation power than the former especially in the representation of derivative functions, e.g. [Le-Cao, Mai-Duy, and Tran-Cong (2009); Mai-Duy and Tran-Cong (2001); Mai-Duy and Tran-Cong (2003)].

In this paper, integrated RBFs (IRBFs) and point collocation are utilised in the context of boundary fitted Cartesian grids and sliding bi-periodic frames for the direct simulation of flows of Newtonian-based particulate systems. The remainder of the paper is organised as follows. Section 2 gives a brief review of the governing equations and the concept of sliding frames. In Section 3, the proposed numerical procedure is described. Numerical results are presented in Section 4. Section 5 concludes the paper.

2   Governing equations and sliding frames concept

2.1   *Governing equations*

Let Π be the entire computational domain, including the interior regions occupied by the particles. Let $P_i(t)$ and $\partial P_i(t)$ be the region and its boundary of the ith particle of time t, where $i = (1, 2, \cdots, N)$ and N is the number of particles (Figure
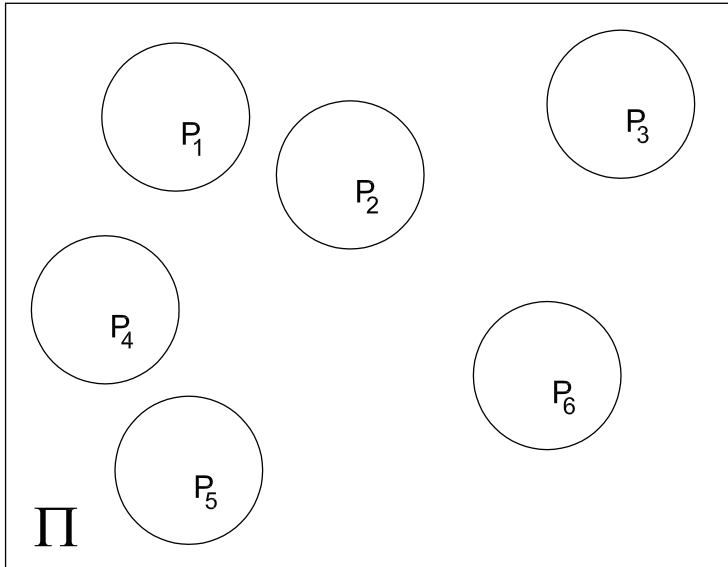
1).

Figure 1: A particle-fluid system

Fluid motion: The laws of mass and momentum conservation for an incompressible fluid lead to

$$\nabla.\mathbf{u} = 0, \tag{1}$$

$$\rho_f \frac{D\mathbf{u}}{Dt} = \nabla.\boldsymbol{\sigma}, \tag{2}$$

where $\mathbf{u}$ is the velocity vector; ρ_f the density of the fluid; $\boldsymbol{\sigma}$ the total stress tensor; and $D[.]/Dt$ the material derivative defined as

$$\frac{D[.]}{Dt} = \frac{\partial[.]}{\partial t} + (\mathbf{u}.\nabla)[.]. \tag{3}$$

For a Newtonian fluid, the total stress tensor is given by

$$\boldsymbol{\sigma} = -p\mathbf{I} + 2\eta\mathbf{D}, \tag{4}$$

where p is the hydrodynamic pressure; $\mathbf{I}$ the unit tensor; η the viscosity; and $\mathbf{D}$ the strain rate tensor defined as

$$\mathbf{D} = \frac{1}{2}[\nabla\mathbf{u} + (\nabla\mathbf{u})^T]. \tag{5}$$

In the case of 2D problems, the stream function - vorticity formulation has been widely employed because of its simplicity. The governing equations (1), (2) and (4) can be rewritten as follows.

$$\frac{\partial^2 \psi}{\partial x^2} + \frac{\partial^2 \psi}{\partial y^2} = \omega, \tag{6}$$

$$\frac{\partial \omega}{\partial t} + u\frac{\partial \omega}{\partial x} + v\frac{\partial \omega}{\partial y} = \frac{1}{Re}\left(\frac{\partial^2 \omega}{\partial x^2} + \frac{\partial^2 \omega}{\partial y^2}\right), \tag{7}$$

where ψ is the stream function; ω the vorticity; Re the Reynolds number; and u and v the components of $\mathbf{u}$, which are defined in terms of the stream function as

$$u = \frac{\partial \psi}{\partial y}, \quad v = -\frac{\partial \psi}{\partial x}.$$

The given velocity boundary conditions, u and v, can be transformed into two boundary conditions on the stream function and its normal derivative

$$\psi = \gamma, \quad \frac{\partial \psi}{\partial n} = \xi,$$

where n is the direction normal to the boundary, and γ and ξ prescribed functions.

Particle motion: Consider an ith particle. The motion of the particle can be described by the Newton-Euler equations

$$M_i\frac{d\mathbf{U}_i}{dt} = \mathbf{F}_i, \tag{8}$$

$$\mathbf{I}_i\frac{d\mathbf{\Omega}_i}{dt} = \mathbf{T}_i, \tag{9}$$

where $M_i, \mathbf{I}_i, \mathbf{U}_i$ and $\mathbf{\Omega}_i$ are the mass, inertia tensor, translational velocity vector of the mass centre and angular velocity vector of the ith particle, respectively; and $\mathbf{F}_i$ and $\mathbf{T}_i$ the force and torque vectors acting on the ith particle.

The force and torque vectors can be computed from the fluid flow as

$$\mathbf{F}_i = \oint_{\partial P_i(t)} \boldsymbol{\sigma}.\mathbf{n}ds, \tag{10}$$

$$\mathbf{T}_i = \oint_{\partial P_i(t)} \mathbf{r} \times (\boldsymbol{\sigma}.\mathbf{n})\,ds, \tag{11}$$

where **r** is the position vector; **n** the outward unit vector normal to the boundary ∂P_i and ds the length of an infinitesimal part of ∂P_i.

Non-slip boundary conditions on the interface between the fluid and the ith particle are given by

$$\mathbf{u} = \mathbf{U}_i + \mathbf{\Omega}_i \times \mathbf{r}, \tag{12}$$

where

$$\mathbf{U}_i = \frac{d\mathbf{X}_i}{dt},$$

$$\mathbf{\Omega}_i = \frac{d\mathbf{\Theta}_i}{dt},$$

in which $\mathbf{X}_i$ is the position vector of the mass center and $\mathbf{\Theta}_i$ the orientation of the ith particle. In terms of the stream function, (12) becomes

$$\frac{\partial \psi}{\partial y} = U_i - \Omega_i y \tag{13}$$

$$\frac{\partial \psi}{\partial x} = -V_i - \Omega_i x, \tag{14}$$

where U_i and V_i are the two components of **U** and Ω_i the magnitude of $\mathbf{\Omega}_i$.

2.2 Sliding bi-periodic frames concept

Consider a particulate flow of very large domain under simple shear conditions in the x direction. One possible way to make such a large problem tractable is to simplify it using the concept of sliding bi-periodic frames. The problem domain can be divided into a set of identical sliding frames of width L and height H (Figure 2). Each frame translates along the shear direction at its own average velocity. Rows of frames slide relatively to one another by an amount $\Delta = \dot{\gamma} H t$, where $\dot{\gamma}$ is the given shear rate, H height of the frame and t shear time [Hwang, Hulsen, and Meijer (2004)].

Because frames have similar solutions, we consider only one frame. If particles in a frame are ignored, it can be seen that the velocity profile is linear

$$u = u_0 + \dot{\gamma} y, \tag{15}$$
$$v = 0, \tag{16}$$

where the origin of the $x - y$ coordinate system is located at the centre of the frame; u_0 the translation velocity of the frame and $-H/2 \le y \le H/2$. With the presence
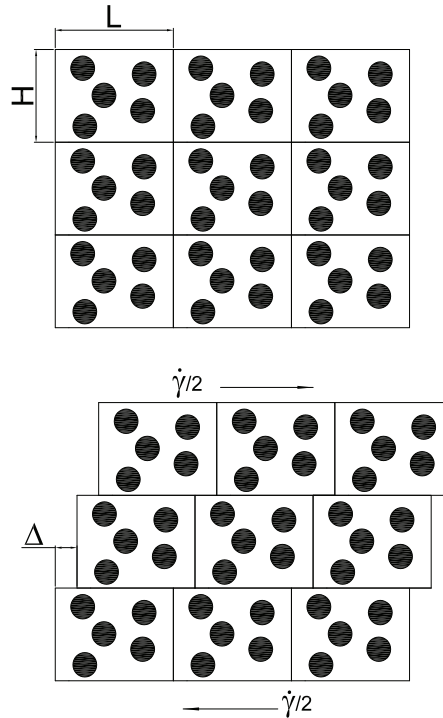
Figure 2: Shear bi-periodic frames.

of particles, one has

$$u = \widehat{u} + u_0 + \dot{\gamma}y, \tag{17}$$
$$v = \widehat{v}, \tag{18}$$

where $\widehat{u}$ and $\widehat{v}$ are the perturbations from the linear profile.

Since the solution is continuous across sliding frames, the following bi-periodic boundary conditions for the velocity $\mathbf{u}$ and the traction $\boldsymbol{\tau}$ can be applied to each frame

$$\mathbf{u}(-L/2, y, t) = \mathbf{u}(L/2, y, t), \quad -H/2 \leq y \leq H/2, \tag{19}$$
$$\boldsymbol{\tau}(-L/2, y, t) = \boldsymbol{\tau}(L/2, y, t), \quad -H/2 \leq y \leq H/2, \tag{20}$$

for the two vertical faces, and

$$\mathbf{u}(x,-H/2,t) = \mathbf{u}(x+\dot{\gamma}Ht,H/2,t) + (\dot{\gamma}H,0)^T, \quad -L/2 \leq x \leq L/2, \tag{21}$$

$$\boldsymbol{\tau}(x,-H/2,t) = \boldsymbol{\tau}(x+\dot{\gamma}Ht,H/2,t), \quad\quad\quad -L/2 \leq x \leq L/2, \tag{22}$$

for the two horizontal faces.

3 Proposed technique

In this study, we propose a numerical procedure based on IRBFs and sliding frames for the simulation of particulate suspensions under simple shear conditions. The fluid domain in a reference frame is simply discretised using a Cartesian grid $n_x \times n_y$. Let $\Gamma_1, \Gamma_2, \Gamma_3$ and Γ_4 be the sides of the reference frame (Figure 3). IRBFs are employed on each grid line to represent the field variables ψ and ω (one-dimensional IRBFs). Sliding bi-periodic boundary conditions are presently implemented by means of point collocation rather than the Lagrange multipliers used in [Hwang, Hulsen, and Meijer (2004)]. The proposed procedure combines strengths of three approaches, namely IRBFs (high-order accuracy), Cartesian grids (easy preprocessing) and the sliding bi-periodic frames concept (infinite number of particles). To our best knowledge, this is a first attempt to use RBFs for the analysis of shear particulate flows. In the following, details are presented for the three constituent components of the proposed procedure. 1D-IRBFs are first described. Sliding bi-periodic boundary conditions are then expressed in terms of the stream function and implemented with IRBFs and point collocation. Finally, suitable formulas and their IRBF implementation are presented for computing the boundary values on the particles.

3.1 1D-IRBFs

Consider a grid line that can be bounded by two faces of the frame, the boundaries of two particles, or the boundary of the particle and the frame. Assume a grid line in the x direction and let f be the field variable. We use IRBFs to approximate f. The construction procedure is as follows.

Second-order derivative of f along a grid line can be decomposed into RBFs

$$\frac{\partial^2 f(x)}{\partial x^2} = \sum_{i=1}^{m} w_i g_i(x) = \sum_{i=1}^{m} w_i I_i^{(2)}(x), \tag{23}$$

where m is the number of RBFs; $\{g_i(x)\}_{i=1}^{m} \equiv \left\{ I_i^{(2)}(x) \right\}_{i=1}^{m}$ the set of RBFs; $\{w_i\}_{i=1}^{m}$ the set of weights to be found and f represents ψ and ω. Approximate expressions

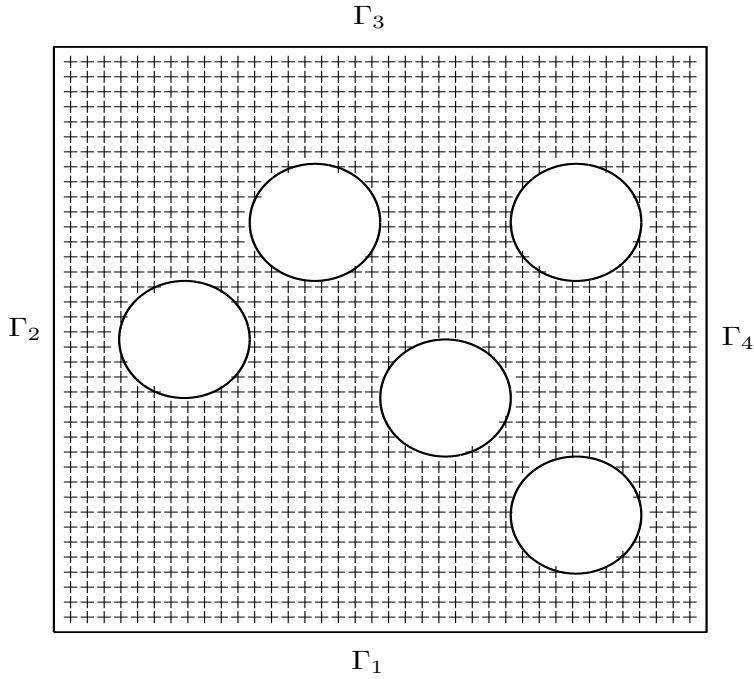Γ_3

Γ_2

Γ_4

Γ_1

Figure 3: A reference frame and its typical Cartesian-grid discretisation.

for the first-order derivative and the field variable are then obtained through integration

$$\frac{\partial f(x)}{\partial x} = \sum_{i=1}^{m} w_i I_i^{(1)}(x) + c_1, \tag{24}$$

$$f(x) = \sum_{i=1}^{m} w_i I_i^{(0)}(x) + c_1 x + c_2, \tag{25}$$

where $I_i^{(1)}(x) = \int I_i^{(2)}(x)dx$ and $I_i^{(0)}(x) = \int I_i^{(1)}(x)dx$. In this study, IRBFs are im-

plemented with the multiquadric (MQ) function and one thus has

$$I_i^{(2)}(x) = \sqrt{(x-c_i)^2 + a_i^2},$$ (26)

$$I_i^{(1)}(x) = \frac{(x-c_i)}{2}A + \frac{a_i^2}{2}B,$$ (27)

$$I_i^{(0)}(x) = \left(\frac{-a_i^2}{3} + \frac{(x-c_i)^2}{6}\right)A + \frac{a_i^2(x-c_i)}{2}B,$$ (28)

where c_i and a_i are the centre and the width of the ith MQ, respectively; $A = \sqrt{(x-c_i)^2 + a_i^2}$; and $B = \ln\left((x-c_i) + \sqrt{(x-c_i)^2 + a_i^2}\right)$. We choose the grid size h as the RBF width a_i. The set of collocation points $\{x_i\}_{i=1}^m$ is taken to be the same as the set of centres $\{c_i\}_{i=1}^m$.
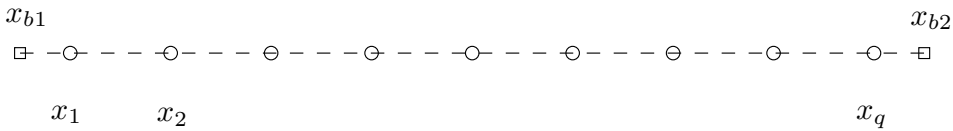
x_{b1} $\qquad\qquad\qquad\qquad\qquad\qquad\qquad\qquad\qquad\qquad\qquad\qquad\quad$ x_{b2}

⊞ ─○─ ─ ─ ─○─ ─ ─ ─ ⊖ ─ ─ ─ ─○ ─ ─ ─ ─○─ ─ ─ ⊖─ ─ ─ ─ ⊖ ─ ─ ─ ─○─ ─ ─ ─○─ ⊟

$\quad\ x_1 \qquad\quad x_2$ $\qquad\qquad\qquad\qquad\qquad\qquad\qquad\qquad\qquad\qquad$ x_q

Figure 4: Nodal points on a grid line consisting of interior points x_i (○) and boundary points x_{bi} (□).

As shown in Figure 4, a grid line contains two sets of nodal points. The first set consists of q interior points that are also the grid nodes (regular nodes). The function values at the interior points $(\{x_i\}_{i=1}^q)$ are unknown. The second set consists of the two nodes x_{b1} and x_{b2} which are generated by the intersection of the grid line and the boundaries.

Collocating (25) at the nodal points yields

$$\begin{pmatrix} \widehat{f} \\ f(x_{b1}) \\ f(x_{b2}) \end{pmatrix} = \widehat{\mathscr{I}}^{(0)} \begin{pmatrix} \widehat{w} \\ c_1 \\ c_2 \end{pmatrix},$$ (29)

where

$$\widehat{f} = (f(x_1), f(x_2), \cdots, f(x_q))^T,$$
$$\widehat{w} = (w_1, w_2, \cdots, w_m)^T,$$

$$\widehat{\mathcal{I}}^{(0)} = \begin{bmatrix} I_1^{(0)}(x_1) & I_2^{(0)}(x_1) & \cdots & I_m^{(0)}(x_1) & x_1 & 1 \\ I_1^{(0)}(x_2) & I_2^{(0)}(x_2) & \cdots & I_m^{(0)}(x_2) & x_2 & 1 \\ \vdots & \vdots & \ddots & \vdots & \vdots & \vdots \\ I_1^{(0)}(x_q) & I_2^{(0)}(x_q) & \cdots & I_m^{(0)}(x_q) & x_q & 1 \\ I_1^{(0)}(x_{b1}) & I_2^{(0)}(x_{b1}) & \cdots & I_m^{(0)}(x_{b1}) & x_{b1} & 1 \\ I_1^{(0)}(x_{b2}) & I_2^{(0)}(x_{b2}) & \cdots & I_m^{(0)}(x_{b2}) & x_{b2} & 1 \end{bmatrix},$$

$$m = q + 2.$$

Solving (29) for the coefficient vector, including the two integration constants, results in

$$\begin{pmatrix} \widehat{w} \\ c_1 \\ c_2 \end{pmatrix} = \left(\widehat{\mathcal{I}}^{(0)} \right)^{-1} \begin{pmatrix} \widehat{f} \\ f(x_{b1}) \\ f(x_{b2}) \end{pmatrix}, \tag{30}$$

where $\left(\widehat{\mathcal{I}}^{(0)} \right)^{-1}$ is the generalised inverse.

Making use of (30), the values of the first and second derivatives of f at the interior points are computed in terms of nodal variable values

$$\begin{pmatrix} \frac{\partial f(x_1)}{\partial x} \\ \frac{\partial f(x_2)}{\partial x} \\ \vdots \\ \frac{\partial f(x_q)}{\partial x} \end{pmatrix} = \widehat{\mathcal{I}}^{(1)} \left(\widehat{\mathcal{I}}^{(0)} \right)^{-1} \begin{pmatrix} \widehat{f} \\ f(x_{b1}) \\ f(x_{b2}) \end{pmatrix}, \tag{31}$$

and

$$\begin{pmatrix} \frac{\partial^2 f(x_1)}{\partial x^2} \\ \frac{\partial^2 f(x_2)}{\partial x^2} \\ \vdots \\ \frac{\partial^2 f(x_q)}{\partial x^2} \end{pmatrix} = \widehat{\mathcal{I}}^{(2)} \left(\widehat{\mathcal{I}}^{(0)} \right)^{-1} \begin{pmatrix} \widehat{f} \\ f(x_{b1}) \\ f(x_{b2}) \end{pmatrix}, \tag{32}$$

where

$$\widehat{\mathscr{I}}^{(1)} = \begin{bmatrix} I_1^{(1)}(x_1) & I_2^{(1)}(x_1) & \cdots & I_m^{(1)}(x_1) & 1 & 0 \\ I_1^{(1)}(x_2) & I_2^{(1)}(x_2) & \cdots & I_m^{(1)}(x_2) & 1 & 0 \\ \vdots & \vdots & \ddots & \vdots & \vdots & \vdots \\ I_1^{(1)}(x_q) & I_2^{(1)}(x_q) & \cdots & I_m^{(1)}(x_q) & 1 & 0 \end{bmatrix},$$

and

$$\widehat{\mathscr{I}}^{(2)} = \begin{bmatrix} g_1(x_1) & g_2(x_1) & \cdots & g_m(x_1) & 0 & 0 \\ g_1(x_2) & g_2(x_2) & \cdots & g_m(x_2) & 0 & 0 \\ \vdots & \vdots & \ddots & \vdots & \vdots & \vdots \\ g_1(x_q) & g_2(x_q) & \cdots & g_m(x_q) & 0 & 0 \end{bmatrix}.$$

It can be seen from (31) and (32) that Dirichlet conditions at x_{b1} and x_{b2} are incorporated into the IRBFN approximations. Depending on how a grid line is bounded, the boundary points x_{b1} and x_{b2} have particular locations. For example, one has $(x_{b1} \in \Gamma_2$ and $x_{b2} \in \Gamma_4)$ if a grid line is bounded by the two vertical faces of the frame, and $(x_{b1} \in \Gamma_2$ and $x_{b2} \in \partial P_i)$ if the boundary surfaces are the left face and the ith particle boundary.

In the same manner, one can obtain the IRBFN expressions for an y grid line.

3.2 Sliding bi-periodic boundary conditions

The continuity of the stream function and the vorticity across two adjacent sliding frames leads to the following periodic boundary conditions [Anderson, Keestra, and Hulsen (2006)]

$$\psi(-L/2, y, t) = \psi(L/2, y, t), \qquad -H/2 \le y \le H/2, \tag{33}$$

$$\frac{\partial \psi}{\partial x}(-L/2, y, t) = \frac{\partial \psi}{\partial x}(L/2, y, t), \quad -H/2 \le y \le H/2, \tag{34}$$

$$\omega(-L/2, y, t) = \omega(L/2, y, t), \qquad -H/2 \le y \le H/2, \tag{35}$$

$$\frac{\partial \omega}{\partial x}(-L/2, y, t) = \frac{\partial \omega}{\partial x}(L/2, y, t), \quad -H/2 \le y \le H/2, \tag{36}$$

for the two vertical faces and

$$\psi(x, -H/2, t) = \psi(x + \dot{\gamma}Ht, H/2, t), \qquad -L/2 \le x \le L/2, \tag{37}$$

$$\frac{\partial \psi}{\partial y}(x, -H/2, t) = \frac{\partial \psi}{\partial y}(x + \dot{\gamma}Ht, H/2, t) + \dot{\gamma}H, \quad -L/2 \le x \le L/2, \tag{38}$$

$$\omega(x, -H/2, t) = \omega(x + \dot{\gamma}Ht, H/2, t), \qquad -L/2 \le x \le L/2, \tag{39}$$

$$\frac{\partial \omega}{\partial y}(x, -H/2, t) = \frac{\partial \omega}{\partial y}(x + \dot{\gamma}Ht, H/2, t), \quad -L/2 \le x \le L/2, \tag{40}$$

for the two horizontal faces.

Consider the stream function ψ. The values of ψ are unknown not only at the interior points (x_i, y_j) with $2 \le i \le n_x - 1$ and $2 \le j \le n_y - 1$ but also at the boundary points of the reference frame $(-L/2, y_j)$, $(L/2, y_j)$, $(x_i, -H/2)$ and $(x_i, H/2)$ with $1 \le j \le n_y$ and $2 \le i \le n_x - 1$. There are $2n_y + 2(n_x - 2)$ unknowns for the latter, leading to $n_{ip} + 2n_y + 2(n_x - 2)$ unknowns in total, where nip is the number of interior points. Apart from collocating the governing equation for ψ at the interior points, one also needs to generate $2n_y + 2(n_x - 2)$ extra equations which can be achieved by using the bi-periodic boundary conditions (33), (34), (37) and (38). Details are as follows.

$$\psi(-L/2, y_j) - \psi(L/2, y_j) = 0, \qquad 1 \le j \le n_y, \tag{41}$$

$$\frac{\partial \psi}{\partial x}(-L/2, y_j) - \frac{\partial \psi}{\partial x}(L/2, y_j) = 0, \quad 1 \le j \le n_y, \tag{42}$$

$$\psi(x_i, -H/2) - \psi(x_i + \dot{\gamma}Ht, H/2) = 0, \qquad 2 \le i \le n_x - 1, \tag{43}$$

$$\frac{\partial \psi}{\partial y}(x_i, -H/2) - \frac{\partial \psi}{\partial y}(x_i + \dot{\gamma}Ht, H/2) - \dot{\gamma}H = 0, \quad 2 \le i \le n_x - 1, \tag{44}$$

where the time variable t is left out for the sake of simplicity.

In (41)-(44), one needs to express $\partial \psi(L/2, y_j)/\partial x$, $\partial \psi(-L/2, y_j)/\partial x$, $\partial \psi(x_i, -H/2)/\partial y$, $\psi(x_i + \dot{\gamma}Ht, H/2)$ and $\partial \psi(x_i + \dot{\gamma}Ht, H/2)/\partial y$ in terms of nodal values of ψ.

For $\partial \psi(\pm L/2, y_j)/\partial x$, the following IRBF expressions are obtained by collocating (24) at $x = \pm L/2$ and then making use of (30)

$$\frac{\partial \psi}{\partial x}(L/2, y_j) = [I_1^{(1)}(L/2), \cdots, I_m^{(1)}(L/2), 1, 0] \left(\widehat{\mathscr{I}}^{(0)} \right)^{-1} \begin{pmatrix} \widehat{\psi} \\ \psi(x_{b1}, y_j) \\ \psi(L/2, y_j) \end{pmatrix}, \tag{45}$$

$$\frac{\partial \psi}{\partial x}(-L/2, y_j) = [I_1^{(1)}(-L/2), \cdots, I_m^{(1)}(-L/2), 1, 0] \left(\widehat{\mathscr{I}}^{(0)} \right)^{-1} \begin{pmatrix} \widehat{\psi} \\ \psi(-L/2, y_j) \\ \psi(x_{b2}, y_j) \end{pmatrix}. \tag{46}$$

Similarly, one can obtain

$$\frac{\partial \psi}{\partial y}(x_i, -H/2) = [I_1^{(1)}(-H/2), \cdots, I_m^{(1)}(-H/2), 1, 0] \left(\widehat{\mathscr{I}}^{(0)} \right)^{-1} \begin{pmatrix} \widehat{\psi} \\ \psi(x_i, -H/2) \\ \psi(x_i, y_{b2}) \end{pmatrix}. \tag{47}$$

For $\psi(x_i + \dot{\gamma}Ht, H/2)$, collocating (25) at $x_i + \dot{\gamma}Ht$ and then making use of (30) lead

to

$$\psi(\bar{x}, H/2) = [I_1^{(0)}(\bar{x}_i), \cdots, I_m^{(0)}(\bar{x}_i), \bar{x}_i, 1] \left(\widehat{\mathscr{I}}^{(0)}\right)^{-1} \begin{pmatrix} \widehat{\psi} \\ \psi(-L/2, H/2) \\ \psi(L/2, H/2) \end{pmatrix}, \quad (48)$$

where $\bar{x}_i = x_i + \dot{\gamma} H t$. The process of deriving the IRBF expression for $\partial \psi(x_i + \dot{\gamma} H t, H/2)/\partial y$ is similar to that for $\psi(x_i + \dot{\gamma} H t, H/2)$.

Sliding bi-periodic boundary conditions for the vorticity are also obtained in a similar fashion.

3.3 Boundary conditions on the particles' boundaries

3.3.1 Boundary conditions for the stream function

The values of the stream function ψ on the boundary of each particle P_i are constant because of $\mathbf{u}(\mathbf{x}).\mathbf{n} = 0$ where $\mathbf{x} \in \partial P_i$ and $\mathbf{n}$ is the outward unit vector normal to ∂P_i. Particles have their own boundary values of ψ which are unknown. To find these unknowns, Lewis (1979) suggested using the condition that the pressure is a single-valued function on the boundary of a particle. This condition can be mathematically described as

$$\oint_{\partial P_i} \frac{\partial p}{\partial s} ds = \oint_{\partial P_i} \nabla p \cdot d\vec{s} = 0, \quad (49)$$

where p is the pressure and s the arc length. In the Cartesian coordinate system, (49) becomes

$$\oint \frac{\partial p}{\partial x} dx + \oint \frac{\partial p}{\partial y} dy = 0. \quad (50)$$

The pressure gradient ∇p can be obtained from the momentum equations in the primitive variable form. By replacing $u = \partial \psi/\partial y$ and $v = -\partial \psi/\partial x$, one can express the components of ∇p in terms of the stream function and its derivatives.

3.3.2 Boundary conditions for the vorticity

The values of the vorticity on ∂P_i can be computed via

$$\omega = \frac{\partial^2 \psi}{\partial x^2} + \frac{\partial^2 \psi}{\partial y^2}, \quad \mathbf{x} \in \partial P_i. \quad (51)$$

The handling of (51) thus involves the evaluation of second-order derivatives of the stream function in both x and y directions. Unfortunately, the boundary points on ∂P_i do not generally coincide with the grid nodes and hence they lie on either

x or *y* grid lines. In [Le-Cao, Mai-Duy, and Tran-Cong (2009)], we proposed the following formulae

$$\omega = \left[1+\left(\frac{t_x}{t_y}\right)^2\right]\frac{\partial^2\psi}{\partial x^2} - \frac{t_x}{t_y^2}\frac{\partial^2\psi}{\partial x\partial s} + \frac{1}{t_y}\frac{\partial^2\psi}{\partial y\partial s}, \quad \mathbf{x}\in\partial P_i, \tag{52}$$

for the *x* grid lines, and

$$\omega = \left[1+\left(\frac{t_y}{t_x}\right)^2\right]\frac{\partial^2\psi}{\partial y^2} - \frac{t_y}{t_x^2}\frac{\partial^2\psi}{\partial y\partial s} + \frac{1}{t_x}\frac{\partial^2\psi}{\partial x\partial s}, \quad \mathbf{x}\in\partial P_i, \tag{53}$$

for the *y* grid lines. In (52) and (53), t_x and t_y are the *x* and *y* components of the unit tangential vector and $\partial(.)/\partial s$ represents the derivative of $(.)$ on ∂P_i which is known (Figure 5). The boundary conditions for the vorticity are thus written in terms of the second derivative of ψ with respect to *x* or *y* only.
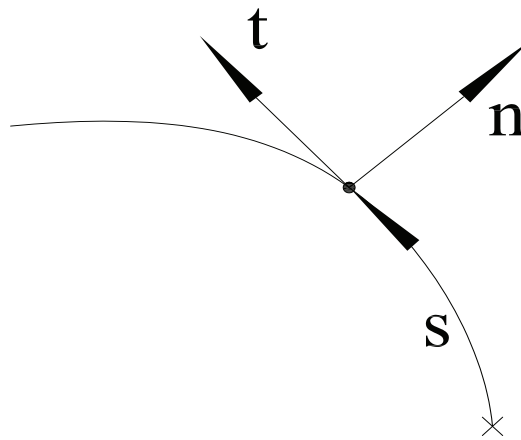

Figure 5: A curved boundary of the particle: arclength, and unit normal and tangential vectors.

In the case that the *i*th particle is of circular shape of radius R_i and rotates about the centre of the reference frame at the angular velocity Ω_i. Expressions for computing

t_x, t_y, $\partial^2 \psi / \partial x \partial s$ and $\partial^2 \psi / \partial y \partial s$ become

$$t_x = \frac{-y}{\sqrt{x^2 + y^2}}, \tag{54}$$

$$t_y = \frac{x}{\sqrt{x^2 + y^2}}, \tag{55}$$

$$\frac{\partial^2 \psi}{\partial x \partial s} = \frac{1}{R_i} \Omega_i y, \tag{56}$$

$$\frac{\partial^2 \psi}{\partial y \partial s} = -\frac{1}{R_i} \Omega_i x. \tag{57}$$

Substitution of (54)-(57) into (52) and (53) yields

$$\omega = \left[1 + \left(\frac{y}{x} \right)^2 \right] \frac{\partial^2 \psi}{\partial x^2} + \left[\left(\frac{y}{x} \right)^2 - 1 \right] \Omega_i, \qquad \mathbf{x} \in \partial P_i, \tag{58}$$

$$\omega = \left[1 + \left(\frac{x}{y} \right)^2 \right] \frac{\partial^2 \psi}{\partial y^2} + \left[\left(\frac{x}{y} \right)^2 - 1 \right] \Omega_i, \quad \mathbf{x} \in \partial P_i. \tag{59}$$

The IRBF implementation of (50) is straightforward, while special treatments are required in handling (52)-(53) and (58)-(59). For the latter, normal derivative boundary conditions for the stream function, i.e. $\partial \psi / \partial n$, need be incorporated into expressions (52), (53), (58) and (59). Since ψ and $\partial \psi / \partial n$ are known from the previous iteration, one can easily obtain the values of $\partial \psi / \partial x$ and $\partial \psi / \partial y$ on ∂P_i. The proposed procedure imposes $\partial \psi / \partial n$, i.e. $\partial \psi / \partial x$ and $\partial \psi / \partial y$, using the constants of integration. On an x grid line, one needs to incorporate $\partial \psi / \partial x$ into $\partial^2 \psi / \partial x^2$, while on an y grid line, $\partial \psi / \partial y$ is incorporated into $\partial^2 \psi / \partial y^2$. Because these two processes are similar, details are given here for an x grid line only, e.g. the one with $x_{b1} \in \Gamma_2$ and $x_{b2} \in \partial P_i$. The system for the conversion of the RBF space into the physical space (29) now takes the form

$$\begin{pmatrix} \widehat{\psi} \\ \psi(x_{b1}) \\ \psi(x_{b2}) \\ \frac{\partial \psi}{\partial x}(x_{b2}) \end{pmatrix} = \begin{pmatrix} \widehat{\mathscr{I}}^{(0)} \\ \mathscr{B} \end{pmatrix} \begin{pmatrix} \widehat{w} \\ c_1 \\ c_2 \end{pmatrix}, \tag{60}$$

where the conversion matrix is of dimensions $(m + 1) \times (m + 2)$ and

$$\mathscr{B} = \left[I_1^{(1)}(x_{b2}), I_2^{(1)}(x_{b2}), \cdots, I_m^{(1)}(x_{b2}), 1, 0 \right].$$

Using (60), one obtains the following from (23) (in which $f \equiv \psi$ and $x \equiv x_{b2}$)

$$\frac{\partial^2 \psi}{\partial x^2}(x_{b2}) = [g_1(x_{b2}), g_2(x_{b2}), \cdots, g_m(x_{b2}), 0, 0] \begin{pmatrix} \widehat{\mathscr{I}}^{(0)} \\ \mathscr{B} \end{pmatrix}^{-1} \begin{pmatrix} \widehat{\psi} \\ \psi(x_{b1}) \\ \psi(x_{b2}) \\ \frac{\partial \psi}{\partial x}(x_{b2}) \end{pmatrix}. \quad (61)$$

Since the conversion matrix in (60) is not over-determined, the IRBFN approximation for $\partial^2 \psi(x_{b2})/\partial x^2$ satisfies $\partial \psi/\partial x$ at $x = x_{b2}$ identically. This imposition shows a clear advantage of IRBFs over the usual differentiated approximations. Substituting (61) into (52), one is able to obtain the boundary conditions on ∂P_i for the vorticity equation. It is noted that given $\partial \psi/\partial x$ and $\partial \psi/\partial y$ on ∂P_i, the terms $\partial^2 \psi/\partial x \partial s$ and $\partial^2 \psi/\partial y \partial s$ in (52) and (53) are known.

4   Numerical examples

In this section, the proposed procedure is validated through three examples. The first example examines the performance of the present technique in the implementation of sliding bi-periodic boundary conditions of the frame. The second example investigates the accuracy of the present technique in the handling of boundary conditions that are similar to those on the particles' boundaries. In the third example, the proposed method is applied to simulate a shear flow of a Newtonian-based particulate system, which is modelled by one particle suspended in a sliding rectangular frame. For all numerical examples, the problem domain is discretised using a uniform Cartesian grid. The interior points that fall very close to the curved/irregular boundary (within a distance of $h/8$, h - the grid size) are removed from the set of nodal points.

4.1   Example 1: Sliding bi-periodic boundary conditions

In this example, the 1D-IRBF implementation of shear bi-periodic boundary conditions is validated. The test problem is governed by

$$\frac{\partial^2 \psi}{\partial x^2} + \frac{\partial^2 \psi}{\partial y^2} = b(x, y). \quad (62)$$

The domain of interest is the region lying between a circle of radius $1/4$ and a square of dimensions 1×1 which are both centered at the origin. The exact solution is

$$\psi(x, y) = \sin(\pi(x - \dot{\gamma} y t)) \sin(\pi y), \quad (63)$$

from which the driving function $b(x,y)$ in (62) and the Dirichlet boundary conditions on the hole can be easily derived. The value of $\dot{\gamma}$ is set to 1. This problem is taken from [Anderson, Keestra, and Hulsen (2006)].

The accuracy of an approximation scheme is measured by means of the discrete relative L_2 error defined as

$$Ne = \frac{\sqrt{\sum_{i=1}^{M}(\psi_i^e - \psi_i)^2}}{\sqrt{\sum_{i=1}^{M}(\psi_i^e)^2}}, \tag{64}$$

where M is the number of unknown nodal values of ψ, and ψ^e and ψ are the exact and approximate solutions, respectively. Another important measure is the convergence rate of the solution with respect to the grid refinement

$$Ne(h) \approx \gamma h^{\alpha} = O(h^{\alpha}), \tag{65}$$

in which α and γ are exponential model's parameters. Given a set of observations, these parameters can be found by the general linear least squares technique.

A number of grids, namely $(12 \times 12, 22 \times 22, \cdots, 62 \times 62)$, are employed for the convergence study. Results concerning the condition number of the system matrix, denoted by cond(A), and the error Ne at $t = 0$ are listed in Table 1. It can be seen that the present system matrix has relatively-low condition numbers and the solution converges fast at the rate of 2.94.

Table 1: Example 1: Errors of the solution and condition numbers of the system matrix. It is noted that $a(b)$ represents $a \times 10^b$.

Grid	*Ne*	Cond(A)
12×12	3.11(-3)	1.6(3)
22×22	4.96(-4)	5.1(3)
32×32	1.52(-4)	1.8(4)
42×42	6.65(-5)	2.2(4)
52×52	3.65(-5)	5.2(4)
62×62	1.98(-5)	5.9(4)

Contour plots for ψ at different values of the shear time t, namely $(0, 0.5, 0.75, 1)$, using a grid of 42×42 are shown in Figure 6. Exact solutions are also included. The two solutions are indistinguishable.

$t = 0$ $t = 0.5$

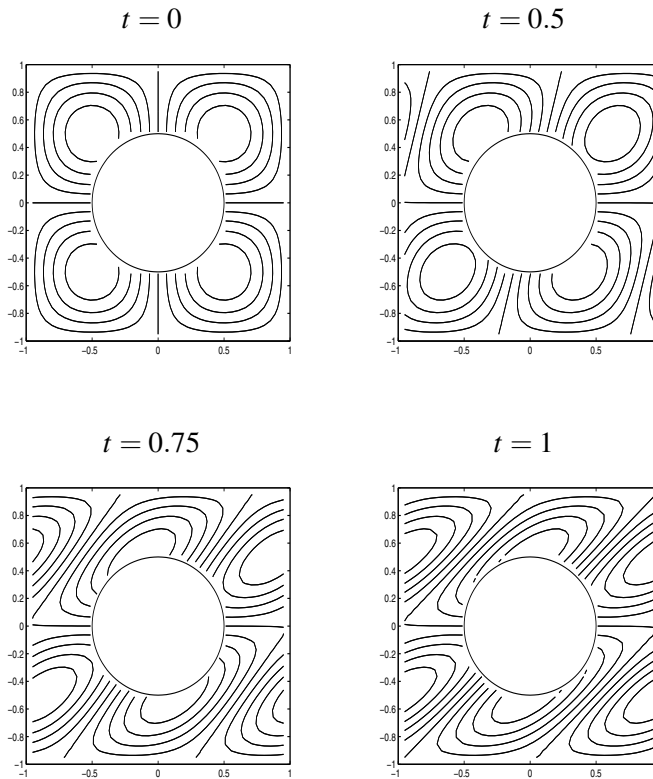$t = 0.75$ $t = 1$

Figure 6: Example 1: Contour plots of the approximate and exact solutions at different time values.

4.2   *Example 2: A rotating circular cylinder*

In this test problem, the 1D-IRBF implementation of boundary conditions of particles is validated through the simulation of the flow of a Newtonian fluid shown in Figure 7. The inner cylinder rotates at a unit angular velocity while the outer cylinder is stationary. The value of ψ on the outer wall is simply set to zero, while the value of ψ on the inner wall is considered as an unknown, denoted by ψ_{wall}. The flow is governed by (6) and (7) and subject to the boundary conditions

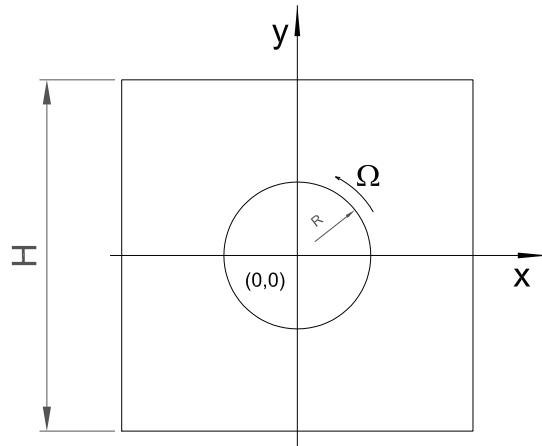$$\psi = \frac{\partial \psi}{\partial x} = \frac{\partial \psi}{\partial y} = 0,$$

Figure 7: Example 2 (rotating cylinder): geometry.

on the outer cylinder and

$$\psi = \psi_{wall}, \quad \frac{\partial \psi}{\partial x} = -x, \quad \frac{\partial \psi}{\partial y} = -y,$$

on the inner cylinder. Using (58) and (59) with $\Omega = 1$, the vorticity boundary values on the rotating cylinder can be computed by

$$\omega = \left[1 + \left(\frac{y}{x}\right)^2\right] \frac{\partial^2 \psi}{\partial x^2} + \left[\left(\frac{y}{x}\right)^2 - 1\right],$$

$$\omega = \left[1 + \left(\frac{x}{y}\right)^2\right] \frac{\partial^2 \psi}{\partial y^2} + \left[\left(\frac{x}{y}\right)^2 - 1\right].$$

The value of ψ_{wall} is found using the single-valued pressure condition as discussed earlier.

The flow is simulated with $R = 0.25$ and $L = 1.0$ using a uniform grid of 36×36. Different values of the Reynolds number, namely (1, 100, 500, 700, 1000), are considered. Results concerning ψ_{wall} obtained by the proposed technique and the finite-difference technique [Lewis (1979)] are presented in Table 2, showing a good agreement. Plots for the velocity vector and vorticity fields for the case of $Re = (1, 700)$ are given in Figure 8.
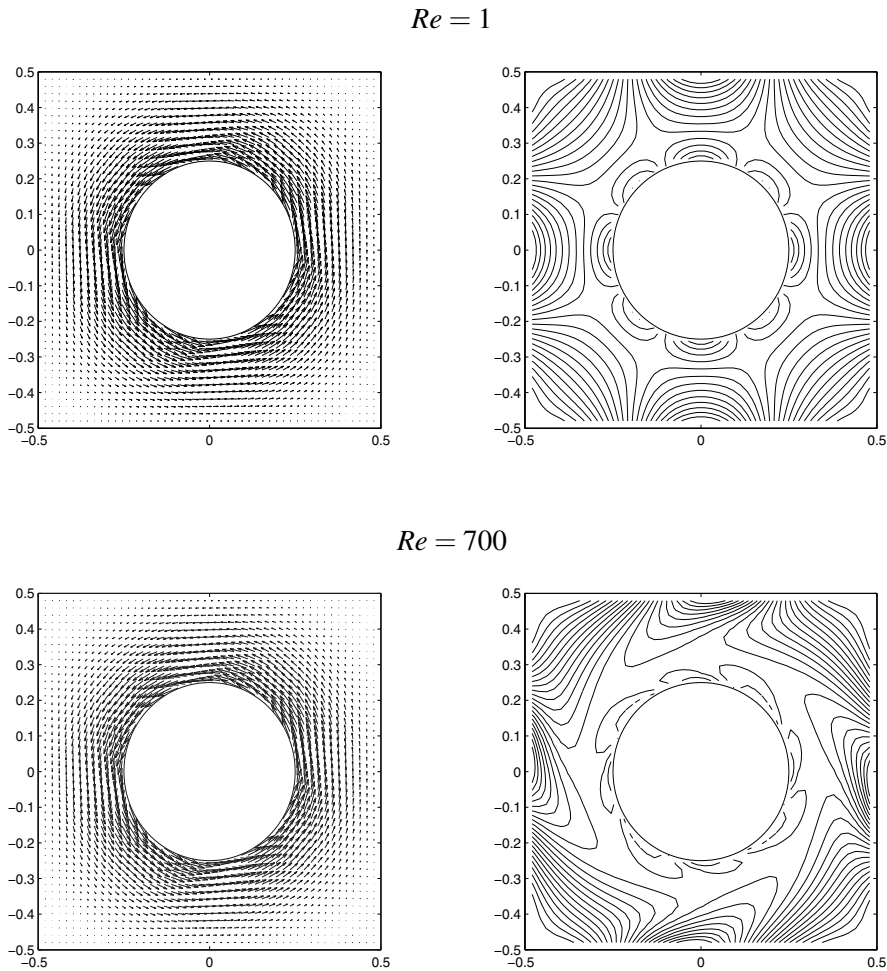
$Re = 1$

$Re = 700$

Figure 8: Example 2: Velocity vector field (left) and vorticity field (right) for the flow at $Re = 1$ and $Re = 700$.

4.3   Example 3: Shear suspension flow

In this example, a single particle of radius R is suspended freely at the center of the reference sliding bi-periodic frame of dimensions 1×1. The fluid domain is the region lying between the particle and the frame (Figure 9). The fluid is Newtonian and moves under a shear rate $\dot{\gamma} = 1$. This configuration can represent the

Table 2: Example 2 (rotating cylinder): Comparison of the stream-function value at the inner cylinder, ψ_{wall}, between the present technique (grid of 36×36) and finite difference technique for different values of *Re*.

Re	100	500	1000
	ψ_{wall}		
Present	0.4637	0.4550	0.4511
[Lewis (1979)]	0.4577	0.4465	0.4375

system of an infinite number of particles as described in Figure 10. It can be seen that the initial configuration is reproduced after the time period $K = 1/\dot{\gamma}$. The inertia of the particle and fluid are ignored. This problem was studied using the fictitious-domain/finite-element method in [Hwang, Hulsen, and Meijer (2004)]. The governing equations for the motion of a fluid thus reduce to

$$\frac{\partial^2 \psi}{\partial x^2} + \frac{\partial^2 \psi}{\partial y^2} = \omega, \tag{66}$$

$$\frac{\partial^2 \omega}{\partial x^2} + \frac{\partial^2 \omega}{\partial y^2} = 0. \tag{67}$$

The boundary conditions of the frame are bi-periodic and determined through (33)-(40), while the boundary conditions of the particle are computed using (50), (58) and (59). However, owing to only one particle considered, the value of ψ on ∂P is simply set to 0. The stress tensor can be written in terms of the stream function and pressure as

$$\boldsymbol{\sigma} = \left[\begin{array}{cc} \left(-p + 2\frac{\partial^2 \psi}{\partial x \partial y}\right) & \left(\frac{\partial^2 \psi}{\partial y^2} - \frac{\partial^2 \psi}{\partial x^2}\right) \\ \left(\frac{\partial^2 \psi}{\partial y^2} - \frac{\partial^2 \psi}{\partial x^2}\right) & \left(-p + 2\frac{\partial^2 \psi}{\partial x \partial y}\right) \end{array} \right]. \tag{68}$$

Conventionally, the interacting hydrodynamic force and moment are first calculated from the fluid flow, and the movement of the particle is then determined from these force and moment using the Newton-Euler equations. Because the inertia of the particle is neglected and there is no external force acting on the particle, the hydrodynamic force and torque are zero (force free and torque free). It can be seen that the particle rotates about the frame centre at the angular velocity Ω and does not translate relative to the frame, i.e. $U = 0$ and $V = 0$. One thus only needs to use the torque-free condition to determine the value of Ω

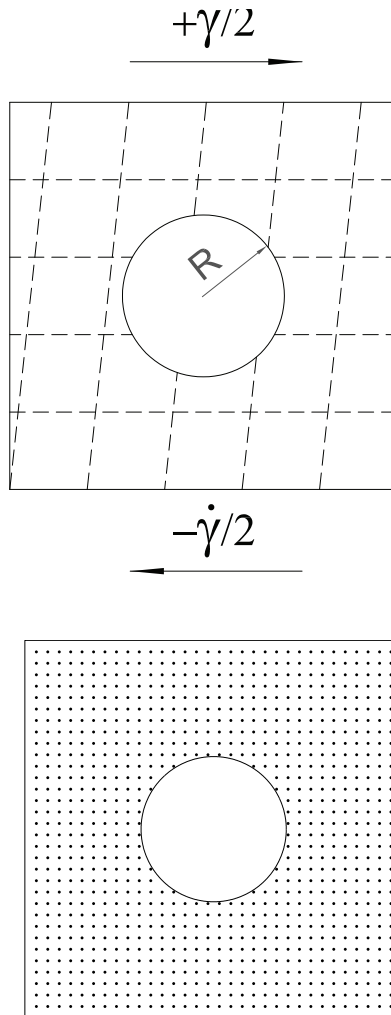$$\mathbf{T} = \int_{\partial P} \mathbf{r} \times (\boldsymbol{\sigma}.\mathbf{n}) \, ds = 0. \tag{69}$$

Figure 9: Example 3: A reference frame (top) and its discretisation (bottom).

The reader is referred to [Hwang, Hulsen, and Meijer (2004)] for further details. Substitution of (68) into (69) yields

$$\oint (x^2 - y^2) \left(\frac{\partial^2 \psi}{\partial y^2} - \frac{\partial^2 \psi}{\partial x^2} \right) ds = 0. \tag{70}$$
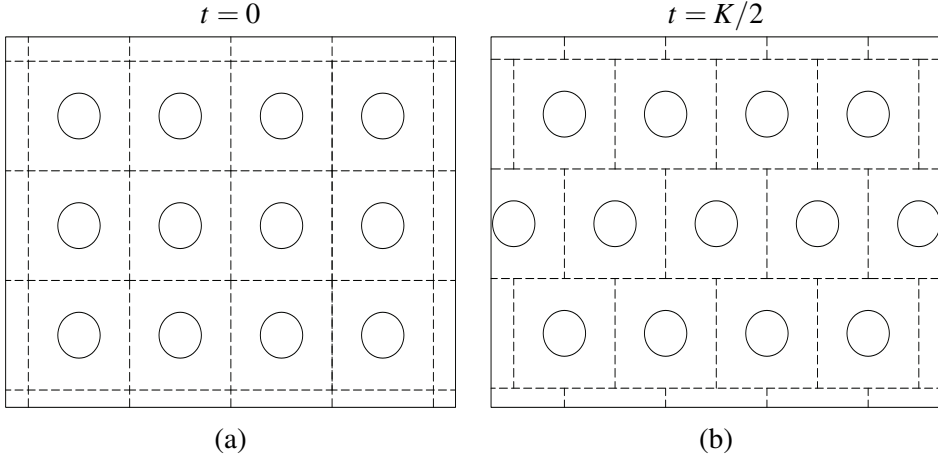
$$t = 0 \qquad\qquad t = K/2$$

(a)   (b)

Figure 10: Example 3: Problem description with two instances during a period of shearing.

In this study, we propose a new way of obtaining Ω. On the particle boundary (Figure 5), one can have

$$\frac{\partial f}{\partial s} = \frac{\partial f}{\partial x} t_x + \frac{\partial f}{\partial y} t_y, \tag{71}$$

where f is a generic function, and s, t_x and t_y are defined as before. By replacing $f = \partial \psi / \partial x$, (71) becomes

$$\frac{\partial^2 \psi}{\partial s \partial x} = \frac{\partial^2 \psi}{\partial x^2} t_x + \frac{\partial^2 \psi}{\partial y \partial x} t_y. \tag{72}$$

Since $U = 0$ and $V = 0$, (13) and (14) reduce to

$$\frac{\partial \psi}{\partial y} = -\Omega y, \tag{73}$$

$$\frac{\partial \psi}{\partial x} = -\Omega x. \tag{74}$$

Substituting (73) and (74) into (72) and making use of $t_x = -y/R$ and $t_y = x/R$ give

$$\Omega = -\frac{\partial^2 \psi}{\partial x^2}. \tag{75}$$

Similarly, by replacing $f = \partial \psi / \partial y$, one has

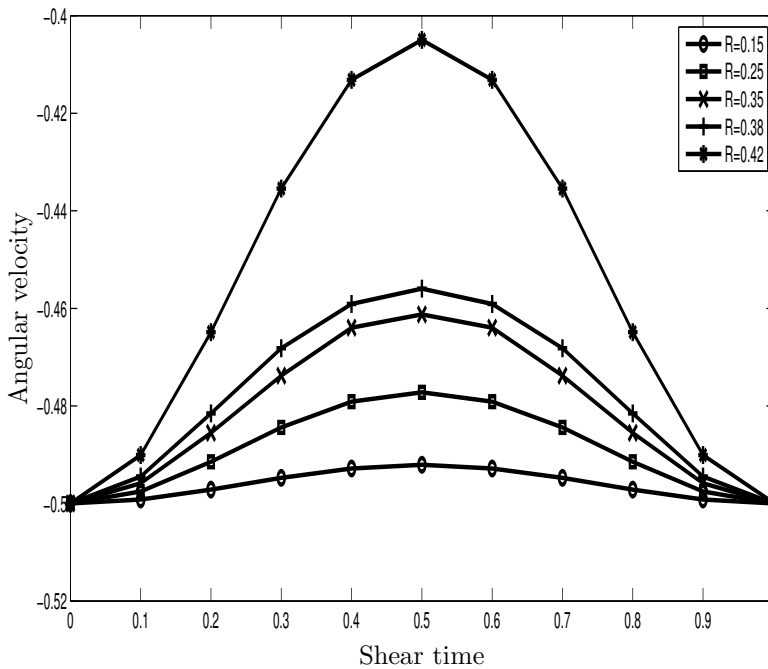$$\Omega = -\frac{\partial^2 \psi}{\partial y^2}. \tag{76}$$

Figure 11: Example 3: Profile of the angular velocity over the period K.

These conditions (75) and (76) can be used as an alternative to (70). In practice, (75) and (76) are applied to the boundary points of the particle on the x and y grid lines, respectively, from which the angular velocity is derived in an average sense.

For each shear interval, the solution procedure is as follows.

1. Guess the distribution of ω and ψ.

2. Discretise (66) and (67) using 1D-IRBFNs. The two system matrices arising from the discretisation of the Laplace operator are identical and remain unchanged during the iteration process.

3. Impose the sliding bi-periodic boundary conditions for ψ and ω on the frame.

4. Derive computational boundary conditions for ω on ∂P.
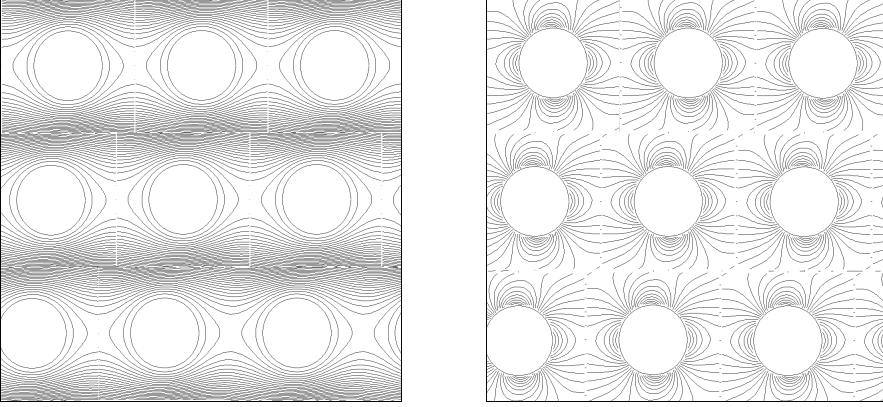
5. Solve (66) for ω and (67) for ψ.

Figure 12: Example 3: Streamlines and iso-vorticity lines at the shear time of 0.3.

6. Compute Ω from (75) and (76).

7. Check the following convergence measure

$$CM = \frac{\sqrt{\sum_{i=1}^{n_{ip}} \left(\psi_i^{(k)} - \psi_i^{(k-1)} \right)^2}}{\sqrt{\sum_{i=1}^{n_{ip}} \left(\psi_i^{(k)} \right)^2}} < \varepsilon,$$

where n_{ip} is the number of interior points, k the current iteration and ε the tolerance. In this study, ε is taken to be 10^{-12}.

8. If not, relax the field solution

$$\psi_i^{(k)} = \alpha \psi_i^{(k)} + (1 - \alpha) \psi_i^{(k-1)},$$

where α is a given number $(0 < \alpha < 1)$, and repeat from step 4. Otherwise, stop the computation and save the results.

The particle's radius R is considered in the range of 0.15 to 0.42. Simulations are carried out using Cartesian grids whose densities vary from 50×50 to 72×72. Denser grids are used for larger values of R.

Figure 11 shows the variation of Ω with respect to the shear time for some different values of R over the period K. It can be seen that the profile of Ω is symmetric
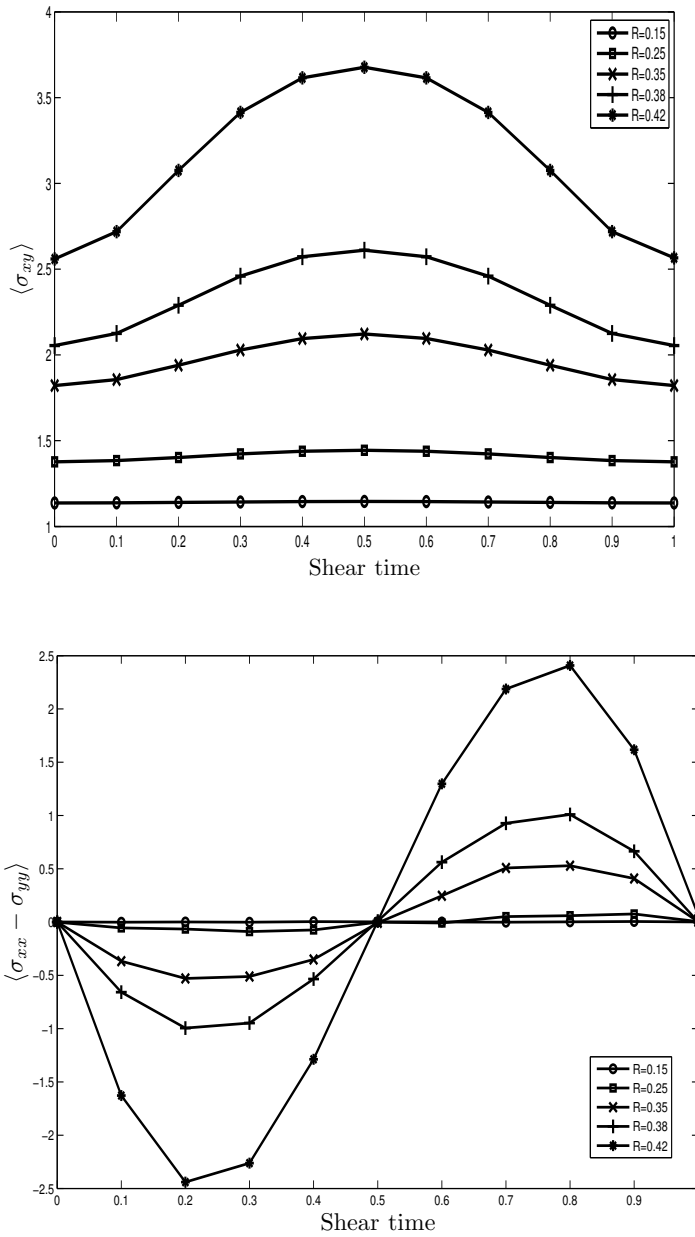
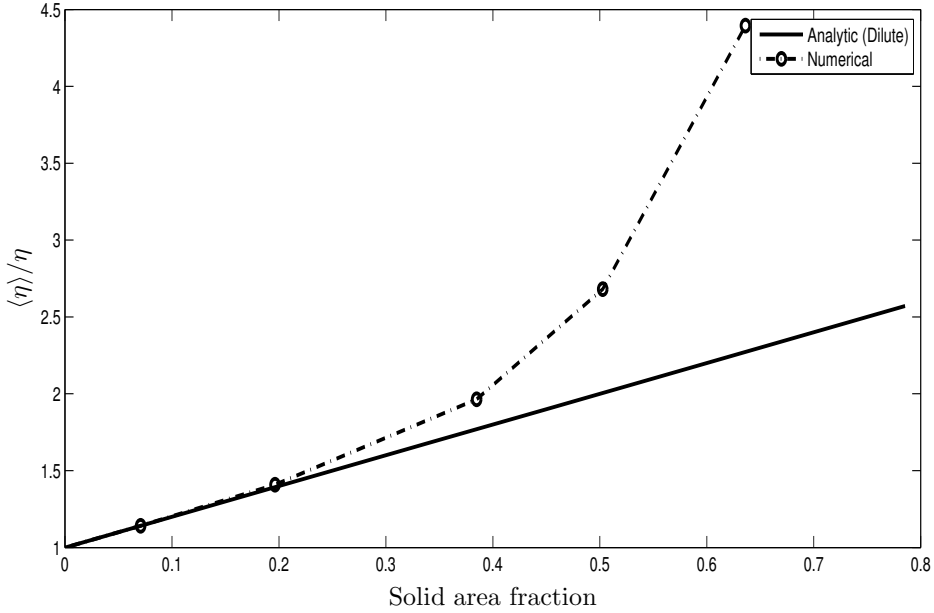Figure 13: Example 3: Variations of the bulk shear and normal stresses over the period *K*.

Figure 14: Example 3: Computed bulk viscosity. Analytic results for the dilute case are also included.

about the vertical line $t = K/2$. The largest value of Ω occurs when the frames line up in the vertical direction (Figure 10a). Furthermore, the fluctuation of Ω is an increasing function of R. In Figure 12, the distribution of ψ and ω over a reference frame are multiplied to produce the ψ and ω fields on the original large domain, where the sliding bi-periodic boundary conditions are clearly observed.

Prediction of the bulk material properties

Following the work of Hwang, Hulsen, and Meijer (2004), the bulk stress can be computed by

$$\langle \boldsymbol{\sigma} \rangle = \frac{1}{A} \int_\Gamma \mathbf{x}\boldsymbol{\tau}^T ds, \tag{77}$$

where $\Gamma = \Gamma_1 \cap \Gamma_2 \cap \Gamma_3 \cap \Gamma_4$ and A is the area of the frame domain, $\mathbf{x}$ the position

vector and $\boldsymbol{\tau}$ the traction vector. In terms of ψ, (77) takes the form

$$\langle \sigma_{xy} \rangle = \frac{1}{A} \int_{\Gamma} y t_x ds = \int_{\Gamma_1} \left(\frac{\partial^2 \psi}{\partial y^2} - \frac{\partial^2 \psi}{\partial x^2} \right) dy, \tag{78}$$

$$\langle \sigma_{xx} \rangle = \frac{1}{A} \int_{\Gamma} x t_x ds = \int_{\Gamma_2} \left(-p + \frac{\partial^2 \psi}{\partial x \partial y} \right) dy + \int_{\Gamma_3} x \left(\frac{\partial^2 \psi}{\partial y^2} - \frac{\partial^2 \psi}{\partial x^2} \right) dx$$

$$- \int_{\Gamma_1} x \left(\frac{\partial^2 \psi}{\partial y^2} - \frac{\partial^2 \psi}{\partial x^2} \right) dx, \tag{79}$$

$$\langle \sigma_{yy} \rangle = \frac{1}{A} \int_{\Gamma} y t_y ds = \frac{1}{2} \int_{\Gamma_3} \left(-p + \frac{\partial^2 \psi}{\partial x \partial y} \right) dx - \frac{1}{2} \int_{\Gamma_1} \left(-p + \frac{\partial^2 \psi}{\partial x \partial y} \right) dx, \tag{80}$$

where the pressure on Γ_2 and Γ_1 are computed using

$$p = \int_{\Gamma_2} \frac{\partial p}{\partial y} dy = - \int_{\Gamma_2} \left(\frac{\partial^3 \psi}{\partial x^3} + \frac{\partial^3 \psi}{\partial y^2 \partial x} \right) dy,$$

$$p = \int_{\Gamma_1} \frac{\partial p}{\partial x} dx = \int_{\Gamma_1} \left(\frac{\partial^3 \psi}{\partial y^3} + \frac{\partial^3 \psi}{\partial x^2 \partial y} \right) dx,$$

and the pressure on Γ_3 is derived from the pressure on Γ_1 and the sliding periodic condition.

Results for the bulk shear stress $\langle \sigma_{xy} \rangle$ and the normal stresses $\langle \sigma_{xx} - \sigma_{yy} \rangle$ are plotted in Figure 13. When the distance between the particles in the sliding frames is maximum (Figure 10b), the bulk shear stress becomes maximum and the bulk normal stress becomes minimum. Both the bulk shear and normal stresses become larger when the particle radius increases and they oscillate with the period K.

The bulk shear viscosity can be obtained by taking the time average of the bulk shear stress over the period K [Hwang, Hulsen, and Meijer (2004)],

$$\frac{\langle \eta \rangle}{\eta} = \frac{1}{K} \int_0^K \langle \sigma_{xy} \rangle dt. \tag{81}$$

In Figure 14, $\langle \eta \rangle / \eta$ is plotted against the solid area fraction ϕ ($\phi = \pi R^2$). In the case of dilute suspensions with circular disks, the bulk shear viscosity can be computed by $\langle \eta \rangle = (1 + 2\phi)\eta$ [Hwang, Hulsen, and Meijer (2004)]. The dilute suspension results are also plotted in Figure 14. It can be seen that the present model produces larger values of $\langle \eta \rangle / \eta$ than the dilute model. This looks reasonable as the present simulations take the interaction between the particles into account.

The observations presented above are similar to those reported in [Hwang, Hulsen, and Meijer (2004)]. Since the finite-element results were presented in graph, we are not able to reproduce them here. However, numerical results by the two techniques appear to be of comparable values, judging from the graphical presentations.

5   Concluding remarks

In this article, a new collocation method based on 1D-IRBFs is developed for the simulation of 2D particulate flows under simple shear conditions. Sliding bi-periodic frames are applied to reduce the large domain to a small one. For the fluid component, the governing equations are taken in the stream function - vorticity formulation and the multiply-connected domain is simply discretised using a Cartesian grid. For the particle component, a new efficient way, based on direct point-wise calculations rather than line/surface integrals, is proposed to compute the angular velocity. Three examples concerning sliding bi-periodic conditions, particle-like boundary conditions and shear particulate suspensions modelled by one particle in each frame are simulated successfully. The presently predicted bulk properties are in good agreement with those by the fictitious-domain/finite-element method.

References

Anderson, P. D.; Keestra, B. J.; Hulsen, M. A. (2006):   On the stream function-vorticity formulation in sliding bi-period frames:application to bulk behavior for polymer blends. *Journal of Computational Physics*, vol. 212, pp. 268–287.

Fasshauer, G. (2007):   *Meshfree Approximation Methods with Matlab*. Interdisciplinary Mathematical Sciences, World Scientific Publishers.

Glowinski, R.; Pan, T. W.; Periaux, J. (1998):   Distributed lagrange multiplier methods for incompressible viscous flow around moving rigid bodies. *Computer Methods in Applied Mechanics and Engineering*, vol. 151(1-2), pp. 181–194.

Hu, H. H. (1995):   Motion of a circular cylinder in a viscous liquid between parallel plates. *Theoretical and Computational Fluid Dynamics*, vol. 7, pp. 441–455.

Hu, H. H.; Joseph, D. D.; Crochet, M. J. (1992):   Direct simulation of fluid particle motions. *Theoretical and Computational Fluid Dynamics*, vol. 3, pp. 285–306.

Huang, P. Y.; Feng, J.; Hu, H. H.; Joseph, D. D. (1997):   Direct simulation of the motion of solid particles in couette and poiseuille flows of viscoelastic fluids. *Journal of Fluid Mechanics*, vol. 343, pp. 73–94.

Huang, P. Y.; Hu, H. H.; Joseph, D. D. (1998): Direct simulation of the sedimentation of elliptic particles in Oldroyd-B fluids. *Journal of Fluid Mechanics*, vol. 362, pp. 297–325.

Hwang, W. R.; Hulsen, M. A.; Meijer, H. E. H. (2004): Direct simulation of particle suspensions in sliding bi-periodic frames. *Journal of Computational Physics*, vol. 194, pp. 742–772.

Kansa, E. J. (1990): Multiquadrics- a scattered data approximation scheme with applications to computational fluid-dynamics-I. surface approximations and partial derivative estimates. *Computers and Mathematics with Applications*, vol. 19(8/9), pp. 127–145.

Le-Cao, K.; Mai-Duy, N.; Tran-Cong, T. (2009): An effective integrated-rbfn cartesian-grid discretization for the stream function-vorticity-temperature formulation in nonrectangular domains. *Numerical Heat Transfer, Part B: Fundamentals*, vol. 55(6), pp. 480–502.

Lees, A. W.; Edwards, S. F. (1972): The computer study of transport processes under extreme conditions. *Journal of Physics C: Solid State Physics*, vol. 5, no. 15, pp. 1921.

Lewis, E. (1979): Steady flow between a rotating circular cylinder and fixed square cylinder. *Journal of Fluid Mechanics*, vol. 95, pp. 497–513.

Mai-Duy, N.; Tran-Cong, T. (2001): Numerical solution of navier-stokes equations using multiquadric radial basis function networks. *International Journal for Numerical Methods in Fluids*, vol. 37 (1), pp. 65–86.

Mai-Duy, N.; Tran-Cong, T. (2003): Approximation of function and its derivatives using radial basis function networks. *Applied Mathematical Modeling*, vol. 27, pp. 197–220.

Patankar, N. A.; Singh, P.; Joseph, D. D.; Glowinski, R.; Pan, T. W. (2000): A new formulation of the distributed lagrange multiplier/ fictitious domain method for particulate flows. *International Journal Multiphase Flow*, vol. 26, pp. 1509–1524.

Phan-Thien, N.; Kim, S. (1994): *Microstructures in Elastic media principles and computational methods*. Oxford University Press.

Sarler, B. (2005): A radial basis function collocation approach in computational fluid dynamics. *CMES: Computer Modeling in Engineering & Sciences*, vol. 7(2), pp. 185–194.

Singh, P.; Joseph, D. D.; Hesla, T. I.; Glowinski, R.; Pan, T. W. (2000): A distributed lagrange multiplier/fictitious domain method for viscoelastic particulate flows. *Journal of Non-Newtonian Fluid Mechanics*, vol. 91, pp. 165–188.